*Yang Xu,
Zhijun Sun,
Shuang Huang,
Xiaowei Sheng,
Xinfu Chi

Dynamic Characteristic Analysis of the Needle Multi-linkage Mechanism in a Carpet Tufting Machine's Driving System

DOI: 10.5604/12303666.1196619

**School of Mechanical Engineering,
Donghua University,**
Shanghai, P. R. China
*E-mail: xuyang@dhu.edu.cn

Abstract
In a typical carpet tufting machine, kinematic and dynamic characteristics of the needle multi-linkage mechanism are the important factors affecting the quality of the tufting carpet. For providing a rational basis for mechanism design and vibration characteristic analysis, a mathematical model of the needle multi-linkage mechanism is constructed using the complex vector analysis method. On the basis of the model, kinematic characteristic curves and dynamic characteristic curves of the needle multi-linkage mechanism are analysed by simulation methods. Finally experimental validation of the alternating load dynamic characteristics is performed on the needle multi-linkage mechanism in a typical carpet tufting machine. The results prove the theoretical analysis validity of the needle multi-linkage mechanism.

Key words: *carpet tufting machine, needle multi-linkage mechanism, kinematic characteristics, dynamic characteristics.*

Introduction

Carpet tufting technology originated in America. Due to low cost and easy-to-develop new varieties, tufted carpet quickly occupied the market from the 1840s, whose production accounted for 80% of the total amount of all kinds of carpets [1 - 3].

The carpet tufting machine is very complex modern textile equipment that can be used to weave all kinds of tufted carpet products. The multi-linkage mechanism is one of the most important parts of the carpet tufting machine's driving system [4 - 9]. Its motion trajectory, displacement, velocity and acceleration determine the quality of the tufting carpet, and the inertial force and inertial torque produced by the multi-linkage mechanisms, which are both an alternating load, will react on the main shaft and cause it to vibrate. Therefore knowing the motion law and alternating load characteristics of the multi-linkage mechanism is very important. Not only can it provide an instruction for the mechanism design of a carpet tufting machine, but also it is the basis for vibration characteristic analysis of the whole mechanical system.

Focusing on a typical tufting machine, its driving system is introduced in this paper. Then the needle multi-linkage mechanism in a carpet tufting machine's driving system is described. A mathematical model of the needle multi-linkage mechanism is constructed using the complex vector analysis method. Kinematic and dynamic characteristics of the needle multi-linkage mechanism are analysed. Motion curves and force curves of the needle multi-linkage mechanism are obtained by simulation methods. Finally the alternating load dynamic characteristics of the needle multi-linkage mechanism were verified by experiment. The results prove the theoretical analysis validity for the needle multi-linkage mechanism.

The tufting carpet machine's driving system

Figure 1 shows a schematic diagram of the typical tufting carpet machine's driving system. In general, the driving system of a typical tufted carpet machine consists of the main shaft, the driven shaft of the needle multi-linkage mechanism, the driven shaft of the hook multi-linkage mechanism, multiple sets of the needle multi-linkage mechanism and multiple sets of the hook multi-linkage mechanism. The needle multi-linkage mechanism and hook multi-linkage mechanism are made up of the driving link and driven link, respectively.

The basic working principle of carpet tufting is shown as follows. Thousands of tufting needles are driven by the main shaft in the carpet tufting machine's driving system to move up and down together. At the same time, the looper hooks the yarn and makes it form a loop on the rear of the backing, coordinating with the tufting needle movement precisely. By controlling the yarn-feeding, different loop heights can be obtained [10, 11].

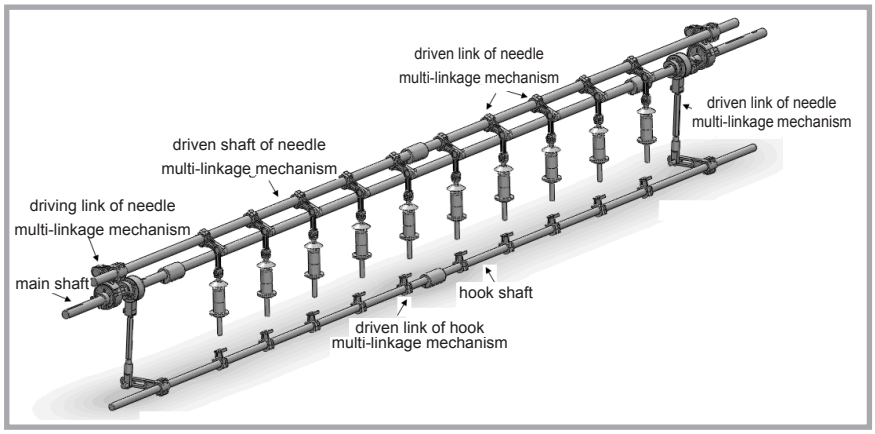

Figure 1. *Schematic diagram of a typical tufting carpet machine's driving system.*

Dynamic model of needle multi-linkage mechanism

Needle multi-linkage mechanism structure

A schematic diagram of the needle multi-linkage mechanism is shown in ***Figure 2***, in which the driving link of the needle multi-linkage mechanism is a crank rocker mechanism containing rod l_1, rod l_2, rod l_3 and a rack, and the driven link of needle multi-linkage mechanism is an offset rocker slider mechanism containing rod l_4, rod l_5 and slider l_6. Rod l_3 and rod l_4 are fixedly connected at joint C and the rod l_4 follows the reciprocating swing of rod l_3. The tufting needle N_1 and N_2 fixedly connected with slider l_6 at point F, and the tufting needle move up and down together with the slider. The role of the needle multi-linkage mechanism is to transform the rotary motion of the main shaft into the vertical reciprocating motion of the tufting needles.

Kinematic model

The basic task of the kinematic mathematical model is to determine the angular displacement θ_i, angular velocity ω_i and angular acceleration a_i of rod l_i (i = 1, 2, ..., 6) in the needle multi-linkage mechanism.

The graphical and complex vector methods are commonly used in kinematic modeling. The graphical method is visualised, but the accuracy is limited, being suitable for analysing the motion of a simple mechanism. The complex vector method has high accuracy and is suitable for analysing the motion of a complex mechanism [12, 13]. In this paper, a kinematic model of the needle multi-linkage mechanism is constructed using the complex vector method. Kinematic models of the crank rocker mechanism and offset rocker slider mechanism in the needle multi-linkage mechanism are respectively constructed as follows:

Kinematic model of the crank rocker mechanism

Figure 3 shows a schematic diagram of the crank rocker mechanism. In ***Figure 3***, l_i represents the rod length, θ_i the angular displacement of rod l_i, x_1 the line distance of OO', and H_1 is the line distance of O'C. Here, i = 1, 2, 3.

According to the closed graph OABCO'O, the real and imaginary parts of the complex vector equation of the crank rocker mechanism are directly listed as ***Equation 1***:

$$\begin{cases} l_1\cos\theta_1 + l_2\cos\theta_2 + l_3\cos(\theta_3 - \pi) - x_1 = 0 \\ l_1\sin\theta_1 + l_2\sin\theta_2 + l_3\sin(\theta_3 - \pi) - H_1 = 0 \end{cases} \quad (1)$$

The equation above is nonlinear and is very difficult to solve. The geometric method is applied for solving the equation. According to the geometric characteristics of triangle ΔOCO', ϕ_1 and l_{OC} can be expressed as:

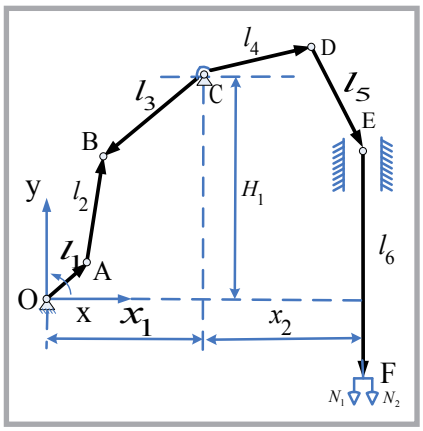

Figure 2. *Schematic diagram of needle multi-linkage mechanism.*

$$\phi_1 = tg^{-1}(x_1 / H_1) \quad (2)$$

$$l_{OC} = \sqrt{H_1^2 + x_1^2} \quad (3)$$

According to the geometric characteristics of triangle ΔAOC, ϕ_2 can be expressed as:

$$\phi_2 = \sin^{-1}\left(\frac{l_1}{l_{AC}} \cdot \sin\phi_4\right) \quad (4)$$

Here, ϕ_4 and l_{AC} can be obtained by:

$$\phi_4 = \frac{\pi}{2} - \phi_1 - \theta_1 \quad (5)$$

$$l_{AC}^2 = l_1^2 + l_{OC}^2 - 2\cdot l_1 \cdot l_{OC} \cdot \cos\phi_4 \quad (6)$$

According to cosine theorem, ϕ_3 can be expressed as:

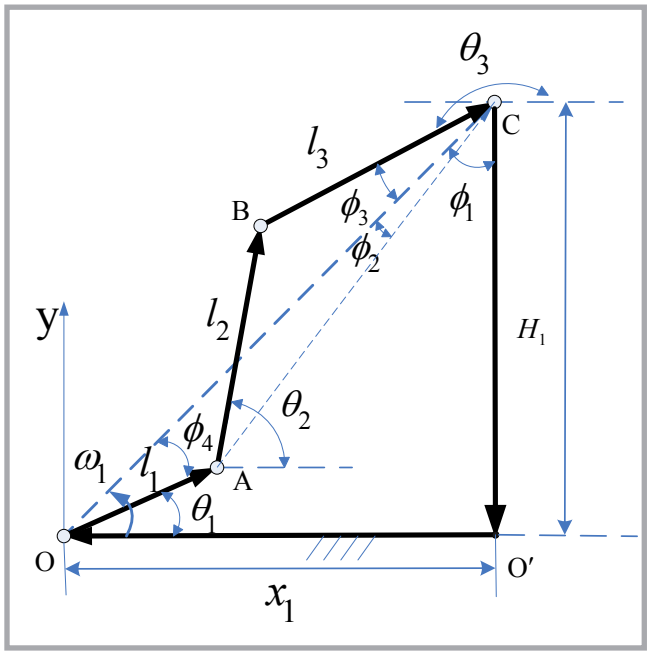

Figure 3. *Schematic diagram of the crank rocker mechanism.*

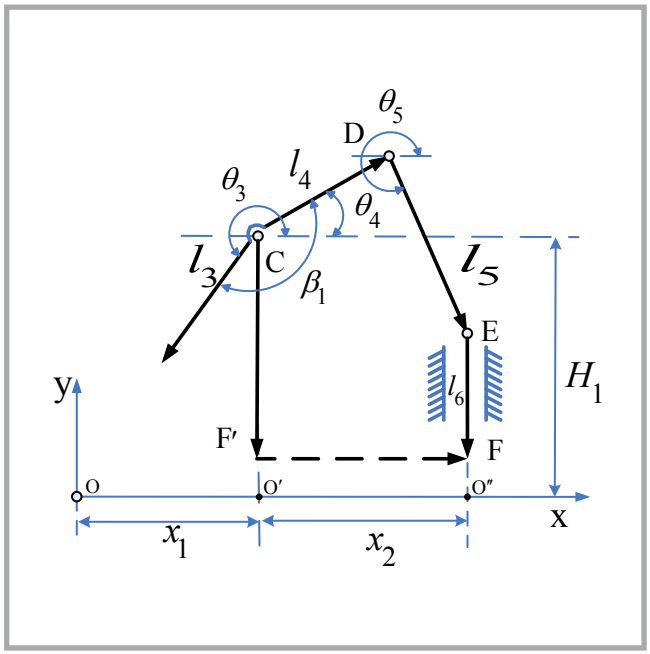

Figure 4. *Schematic diagram of the offset rocker slider mechanism.*

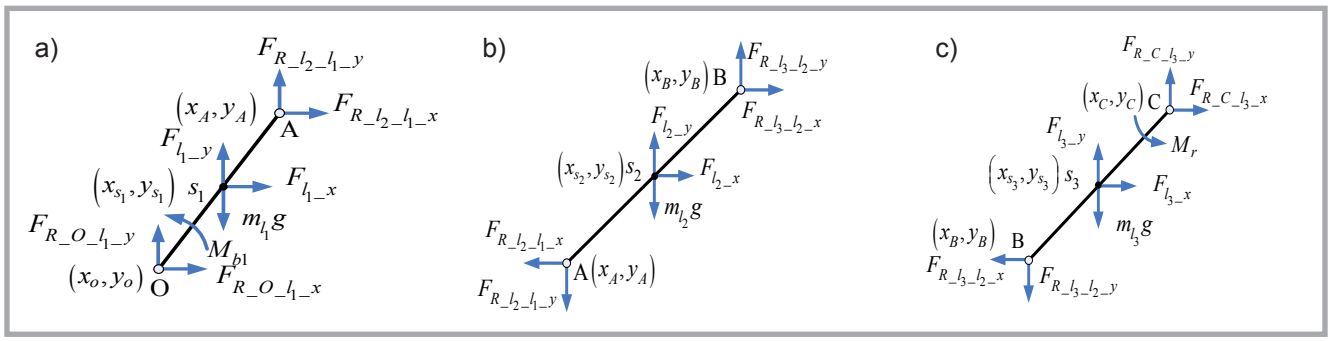

Figure 5. *Force analysis diagram for the crank rocker mechanism; a) force analysis diagram for rod l_1, b) force analysis diagram for rod l_2, c) force analysis diagram for rod l_3.*

$$\phi_3 = \cos^{-1}\left(\frac{l_{AC}^2 + l_3^2 - l_2^2}{2 \cdot l_{AC} \cdot l_3}\right) - \phi_2 \quad (7)$$

Therefore, the rotary angle θ_3 of rod l_3 can be derived as follows:

$$\theta_3 = \frac{3\pi}{2} - \phi_1 - \phi_3 \quad (8)$$

From ***Equation 1***, the rotary angle θ_2 of rod l_2 can be expressed as:

$$\theta_2 = \sin^{-1}\left(\frac{l_3 \sin\theta_3 - l_1 \sin\theta_1 + H_1}{l_2}\right) \quad (9)$$

Taking the first derivative of ***Equation 1***, the angular velocities ω_2 and ω_3 of rods l_2 and l_3 can be obtained as follows, respectively.

$$\omega_2 = -\frac{l_1\omega_1 \sin(\theta_1 - \theta_3)}{l_2 \sin(\theta_2 - \theta_3)} \quad (10)$$

$$\omega_3 = \frac{l_1\omega_1 \sin(\theta_1 - \theta_2)}{l_3 \sin(\theta_3 - \theta_2)} \quad (11)$$

Taking the second derivative of ***Equation 1***, the angular accelerations a_2 and a_3 of rod l_2 and rod l_3 can be derived as follows, respectively.

$$a_2 = \frac{l_3\omega_3^2 - l_1\omega_1^2 \cos(\theta_1 - \theta_3) - l_2\omega_2^2 \cos(\theta_2 - \theta_3)}{l_2 \sin(\theta_2 - \theta_3)} \quad (12)$$

$$a_3 = \frac{l_2\omega_2^2 + l_1\omega_1^2 \cos(\theta_1 - \theta_2) - l_3\omega_3^2 \cos(\theta_3 - \theta_2)}{l_3 \sin(\theta_3 - \theta_2)} \quad (13)$$

Kinematic model of the offset rocker slider mechanism

Figure 4 shows a schematic diagram of the offset rocker slider mechanism. In ***Figure 4***, l_i and θ_i represent the same as those of the crank rocker mechanism. Here, i = 4, 5. x_2 is the line distance of $O'O''$.

According to the closed graph CDEFC, the real and imaginary parts of the complex vector equation of the offset rocker slider mechanism can be obtained as follows:

$$\begin{cases} \theta_5 = \cos^{-1}\left(\dfrac{x_2 - l_4\cos\theta_4}{l_5}\right) \\ l_{CF'} = l_6 - l_4\sin\theta_4 - l_5\sin\theta_5 \end{cases} \quad (14)$$

According to the intersection angle β_1 of rods and l_4, the angle θ_4 of rod l_4 can be expressed as follows:

$$\theta_4 = \theta_3 + \beta_1 - 2\pi \quad (15)$$

Because rods l_3 and rod l_3 are fixedly connected at joint C, the angular velocities and angular acceleration of rods l_3 and l_4 should be equal, and thus, $\omega_4 = \omega_3$, $a_4 = a_3$. Taking the first derivative of ***Equation 14***, the angular velocity ω_5 of rod l_5 and linear velocity $v_{CF'}$ of slider l_6 can be derived as follows, respectively.

$$\omega_5 = -\frac{l_4\omega_4 \sin\theta_4}{l_5 \sin\theta_5} \quad (16)$$

$$v_{CF'} = -l_4\omega_4 \cos\theta_4 - -l_5\omega_5 \cos\theta_5 \quad (17)$$

Taking the second derivative of ***Equation 14***, the angular acceleration a_5 of rod l_5 and linear acceleration $a_{CF'}$ of slider l_6 can be derived as follows, respectively.

$$a_5 = -\frac{(l_4 a_4 \sin\theta_4 + l_4\omega_4^2 \cos\theta_4 + l_5\omega_5^2 \cos\theta_5)}{l_5 \sin\theta_5} \quad (18)$$

$$a_{CF'} = -(l_4 a_4 \cos\theta_4 - l_4\omega_4^2 \sin\theta_4 + l_5 a_5 \cos\theta_5 - l_5\omega_5^2 \sin\theta_5) \quad (19)$$

Dynamic model

The basis task of dynamic analysis is to analyse the inertial force and inertial torque produced by the needle multi-linkage mechanism. In this section, dynamic models of the crank rocker and offset rocker slider mechanisms in the needle multi-linkage mechanism are respectively constructed as follows.

Dynamic model of the crank rocker mechanism

Figure 5 shows a force analysis diagram for the crank rocker mechanism. In ***Figure 5***, x_{s_i} and y_{s_i} represent the horizontal ordinate and the vertical coordinate of rod centroid s_i. x_z respectively, and y_z the horizontal ordinate and vertical coordinate of joint z (z = O, A, B, C). m_{l_i} is the mass of rod l_i. $F_{l_i\_x}$ and $F_{l_i\_y}$ represent the X direction inertial forces and those of the Y directions of rod l_i. M_i represents the inertial torque of rod l_i. $F_{R\_z\_l_i\_x}$ and $F_{R\_z\_l_i\_y}$ represent the X direction's reaction force and Y direction's reaction force, respectively, which joint z gives to rod . $F_{R\_l_i\_l_j\_x}$ and $F_{R\_l_i\_l_j\_y}$ represent the X direction's reaction force and the Y direction's reaction force, respec-

$$\begin{cases} F_{R\_l_2\_l_1\_x} + F_{R\_O\_l_1\_x} = -F_{l_1\_x} \\ F_{R\_l_2\_l_1\_y} + F_{R\_O\_l_1\_y} - m_{l_1}g = -F_{l_1\_y} \\ M_b + F_{R\_O\_l_1\_x}(y_{s1} - y_o) + F_{R\_l_2\_l_1\_y}(x_A - x_{s1}) - F_{R\_l_2\_l_1\_x}(y_A - y_{s1}) - F_{R\_O\_l_1\_y}(x_{s1} - x_o) = -M_1 = 0 \end{cases} \quad (22)$$

$$\begin{cases} F_{R\_l_3\_l_2\_x} - F_{R\_l_2\_l_1\_x} = -F_{l_2\_x} \\ F_{R\_l_3\_l_2\_y} - F_{R\_l_2\_l_1\_y} - m_{l_2}g = -F_{l_2\_y} \\ F_{R\_l_3\_l_2\_x}(y_{s2} - y_B) + F_{R\_l_3\_l_2\_y}(x_B - x_{s2}) + F_{R\_l_2\_l_1\_x}(y_A - y_{s2}) + F_{R\_l_2\_l_1\_y}(x_{s2} - x_A) = -M_2 \end{cases} \quad (25)$$

Equations 22 & 25.

$$\begin{cases} F_{R\_C\_l_3\_x} - F_{R\_l_3\_l_2\_x} = -F_{l_3\_x} \\ F_{R\_C\_l_3\_y} - F_{R\_l_3\_l_2\_y} - m_{l_3} g = -F_{l_3\_y} \\ M_r + F_{R\_C\_l_3\_y}(x_C - x_{s3}) + F_{R\_l_3\_l_2\_y}(x_{s3} - x_B) - F_{R\_C\_l_3\_x}(y_C - y_{s3}) - F_{R\_l_3\_l_2\_x}(y_{s3} - y_B) = -M_3 \end{cases} \quad (28)$$

$$A = \begin{bmatrix} 1 & 0 & 1 & 0 & 0 & 0 & 0 & 0 & 0 \\ 0 & 1 & 0 & 1 & 0 & 0 & 0 & 0 & 0 \\ -(y_A - y_{s1}) & (x_A - x_{s1}) & (y_{s1} - y_o) & -(x_{s1} - x_o) & 0 & 0 & 0 & 0 & 1 \\ -1 & 0 & 0 & 0 & 1 & 0 & 0 & 0 & 0 \\ 0 & -1 & 0 & 0 & 0 & 1 & 0 & 0 & 0 \\ (y_A - y_{s2}) & (x_{s2} - x_A) & 0 & 0 & (y_{s2} - y_B) & (x_B - x_{s2}) & 0 & 0 & 0 \\ 0 & 0 & 0 & 0 & -1 & 0 & 1 & 0 & 0 \\ 0 & 0 & 0 & 0 & 0 & -1 & 0 & 1 & 0 \\ 0 & 0 & 0 & 0 & -(y_{s3} - y_B) & (x_{s3} - x_B) & -(y_C - y_{s3}) & (x_C - x_{s3}) & 0 \end{bmatrix} \quad (30)$$

$$F_{R1} = \begin{bmatrix} F_{R\_l_2\_l_1\_x} & F_{R\_l_2\_l_1\_y} & F_{R\_O\_l_1\_x} & F_{R\_O\_l_1\_y} & F_{R\_l_3\_l_2\_x} & F_{R\_l_3\_l_2\_y} & F_{R\_C\_l_3\_x} & F_{R\_C\_l_3\_y} & M_{b1} \end{bmatrix}^T \quad (31)$$

$$B = \begin{bmatrix} -F_{l_1\_x} & -F_{l_1\_y} + m_{l_1} g & 0 & -F_{l_2\_x} & -F_{l_2\_y} + m_{l_2} g & -M_2 & -F_{l_3\_x} & -F_{l_3\_y} + m_{l_3} g & -M_3 - M_r \end{bmatrix}^T \quad (32)$$

$$\begin{cases} F_{R\_l_5\_l_4\_x} + F_{R\_C\_l_4\_x} = -F_{l_4\_x} \\ F_{R\_l_5\_l_4\_y} + F_{R\_C\_l_4\_y} - m_{l_4} g = -F_{l_4\_y} \\ M_r + F_{R\_l_5\_l_4\_x}(y_D - y_{s4}) + F_{R\_C\_l_4\_y}(x_{s4} - x_C) - F_{R\_l_5\_l_4\_y}(x_D - x_{s4}) - F_{R\_C\_l_4\_x}(y_{s4} - y_C) = -M_4 \end{cases} \quad (35)$$

$$\begin{cases} F_{R\_l_6\_l_5\_x} - F_{R\_l_5\_l_4\_x} = -F_{l_5\_x} \\ F_{R\_l_6\_l_5\_y} - F_{R\_l_5\_l_4\_y} - m_{l_5} g = -F_{l_5\_y} \\ F_{R\_l_6\_l_5\_x}(y_{s5} - y_E) + F_{R\_l_6\_l_5\_y}(x_E - x_{s5}) + F_{R\_l_5\_l_4\_x}(y_D - y_{s5}) + F_{R\_l_5\_l_4\_y}(x_{s5} - x_D) = -M_5 \end{cases} \quad (38)$$

Equations 28, 30, 31, 32, 35 & 38.

tively, which rod l_i gives to rod l_j. M_r and M_{b1} are, respectively, the resistance torque and balancing torque of the crank rocker mechanism. Here, $i = 1, 2, 3$.

Based on the complex vector method, the acceleration of centroid s_1 can be expressed as follows:

$$\begin{cases} a_{s1x} = -\frac{l_1}{2}\omega_1^2 \cos\theta_1 \\ a_{s1y} = -\frac{l_1}{2}\omega_1^2 \sin\theta_1 \end{cases} \quad (20)$$

From ***Figure 5.a***, the inertial force and inertial moment of rod l_1 can be determined as:

$$\begin{cases} F_{l_1\_x} = -m_{l_1} a_{s1x} \\ F_{l_1\_y} = -m_{l_1} a_{s1y} \\ M_1 = -J_{s1} a_1 \end{cases} \quad (21)$$

The force balance equation of rod l_1 can be expressed as ***Equation 22*** (see page 105).

Similarly the force balance equations of l_2 and l_3 can be obtained as follows according to ***Figures 5.b*** and ***5.c***.

$$\begin{cases} a_{s2x} = -l_1\omega_1^2 \cos\theta_1 - \frac{l_2}{2}\omega_2^2 \cos\theta_2 - \frac{l_2}{2} a_2 \sin\theta_2 \\ a_{s2y} = -l_1\omega_1^2 \sin\theta_1 - \frac{l_2}{2}\omega_2^2 \sin\theta_2 + \frac{l_2}{2} a_2 \cos\theta_2 \end{cases} \quad (23)$$

$$\begin{cases} F_{l_2\_x} = -m_{l_2} a_{s2x} \\ F_{l_2\_y} = -m_{l_2} a_{s2y} \\ M_2 = -J_{s2} a_2 \end{cases} \quad (24)$$

Equation 25 (see page 105)

$$\begin{cases} a_{s3x} = -\frac{l_3}{2}\left(\omega_3^2 \cos\theta_3 + a_3 \sin\theta_3\right) \\ a_{s3y} = -\frac{l_3}{2}\left(\omega_3^2 \sin\theta_3 - a_3 \cos\theta_3\right) \end{cases} \quad (26)$$

$$\begin{cases} F_{l_3\_x} = -m_{l_3} a_{s3x} \\ F_{l_3\_y} = -m_{l_3} a_{s3y} \\ M_3 = -J_{s3} a_3 \end{cases} \quad (27)$$

Combining ***Equation 20*** with ***Equation 28***, a matrix equation can be obtained as follows:

$$AF_{R1} = B \quad (29)$$

Here, A is the coefficient of the matrix, F_{R1} the unknown force matrix of the crank rocker mechanism, and B is the known force matrix of the crank rocker mechanism.

Dynamic model of the offset rocker slider mechanism

Figure 6 shows a force analysis diagram for the offset rocker slider mechanism. In ***Figure 6***, F_r is the friction force of slider l_6 when the tufting needle stabs into the backing. Other symbols are of the same meaning as for the crank rocker mechanism. Here, $i = 4, 5, 6$.

According to ***Figures 6.a*** and ***6.b***, the force balance equations of l_4 and l_5 can be respectively expressed as follows.

$$\begin{cases} a_{s4x} = -\frac{l_4}{2}\omega_4 \cos\theta_4 - \frac{l_4}{2} a_4 \sin\theta_4 \\ a_{s4y} = -\frac{l_4}{2}\omega_4 \sin\theta_4 + \frac{l_4}{2} a_4 \cos\theta_4 \end{cases} \quad (33)$$

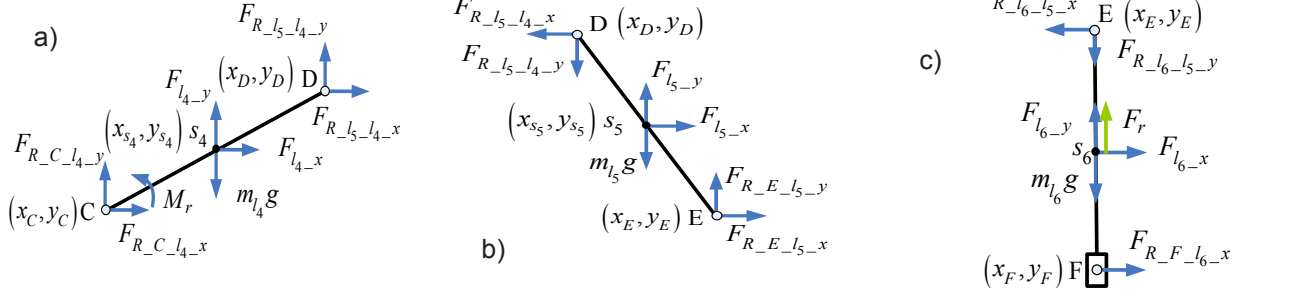

Figure 6. *Force analysis diagram for the offset rocker slider mechanism; a) Force analysis diagram for rod l_4, b) Force analysis diagram for rod l_5, c) Force analysis diagram for slider l_6 when the tufting needle moves down.*

$$\begin{cases} F_{l_4\_x} = -m_{l_4} a_{s4x} \\ F_{l_4\_y} = -m_{l_4} a_{s4y} \\ M_4 = -J_{s4} a_4 \end{cases} \quad (34)$$

$$\begin{cases} a_{s5x} = -l_4\omega_4^2 \cos\theta_4 - l_4 a_4 \sin\theta_4 - \frac{l_5}{2}\omega_5^2 \cos\theta_5 - \frac{l_5}{2} a_5 \sin\theta_5 \\ a_{s5y} = -l_4\omega_4^2 \sin\theta_4 + l_4 a_4 \cos\theta_4 - \frac{l_5}{2}\omega_5^2 \sin\theta_5 + \frac{l_5}{2} a_5 \cos\theta_5 \end{cases} \quad (36)$$

$$\begin{cases} F_{l_5\_x} = -m_{l_5} a_{s5x} \\ F_{l_5\_y} = -m_{l_5} a_{s5y} \\ M_5 = -J_{s5} a_5 \end{cases} \quad (37)$$

According to Figure 6c), the force balance equations of slider l_6 when the tufting needle moves down can be given by:

$$\begin{cases} F_{R\_l_6\_l_5\_x} - F_{R\_F\_l_6} = -F_{l_6\_x} \\ m_{l_6} g - F_r + F_{R\_l_6\_l_5\_y} = F_{l_6\_y} \end{cases} \quad (39)$$

When the tufting needle moves up, F_r in the equation above is the reverse. Other parameters remain unchanged.

Combining ***Equation 33*** with ***Equation 39***, a matrix equation can be obtained as follows:

$$CF_{R2} = D \quad (40)$$

Where, C is the coefficient of the matrix. F_{R2} the unknown force matrix of the offset slider mechanism, and D is the known force matrix of the offset slider mechanism (see ***Equations 41, 42 & 43***).

$$C = \begin{bmatrix} 1 & 0 & 1 & 0 & 0 & 0 & 0 & 0 \\ 0 & 1 & 0 & 1 & 0 & 0 & 0 & 0 \\ -(y_{s4} - y_C) & (x_{s4} - x_C) & (y_D - y_{s4}) & -(x_D - x_{s4}) & 0 & 0 & 0 & 1 \\ 0 & 0 & -1 & 0 & 1 & 0 & 0 & 0 \\ 0 & 0 & 0 & -1 & 0 & 1 & 0 & 0 \\ 0 & 0 & (y_D - y_{s5}) & -(x_D - x_{s5}) & (y_{s5} - y_E) & -(x_{s5} - x_E) & 0 & 0 \\ 0 & 0 & 0 & 0 & -1 & 0 & 1 & 0 \\ 0 & 0 & 0 & 0 & 0 & -1 & 0 & 0 \end{bmatrix} \quad (41)$$

$$F_{R2} = \begin{bmatrix} F_{R\_C\_l_4\_x} & F_{R\_C\_l_4\_y} & F_{R\_l_5\_l_4\_x} & F_{R\_l_5\_l_4\_y} & F_{R\_l_6\_l_5\_x} & F_{R\_l_6\_l_5\_y} & F_{R\_F\_l_6\_x} & M_r \end{bmatrix}^T \quad (42)$$

$$D = \begin{bmatrix} -F_{l_4\_x} & -F_{l_4\_y} + m_{l_4} g & -M_4 & -F_{l_5\_x} & -F_{l_5\_y} + m_{l_5} g & -M_5 & 0 & -F_{l_6\_y} - F_r + m_{l_6} g \end{bmatrix}^T \quad (43)$$

Equations 41, 42 & 43.

Table 1. *Main parameters of the needle multi-linkage mechanism.*

Link parameter	Material	Length, mm	Mass, kg	Moment of inertia, × 10^{-3} kg·m^2
l_1	cast steel	15	3.07	4.34
l_2		138	3.79	26.99
l_3		115	2.96	10.77
l_4		125	1.74	6.69
l_5		120	0.36	0.91
l_6		440	1.47	19.15
x_1	—	70	—	—
x_2		100		
H_1		155		

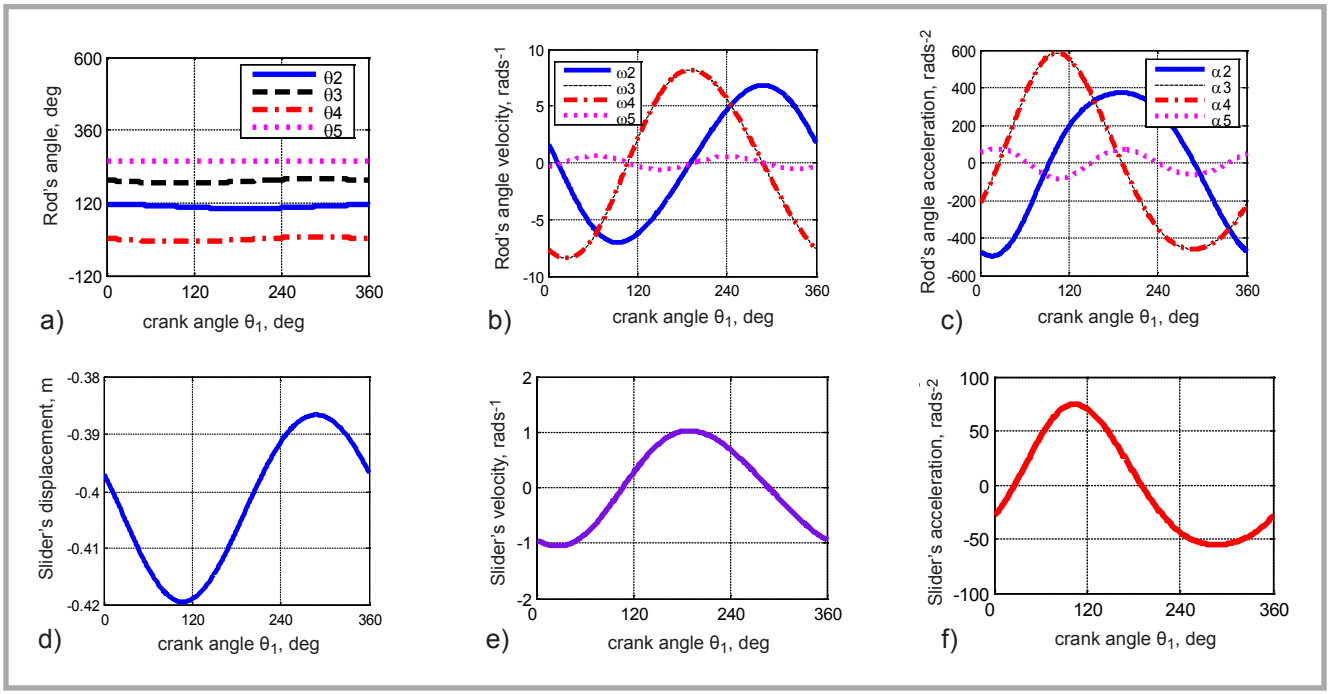

Figure 7. *Motion curves of needle multi-linkage mechanism; a) rod's angle displacement curves, b) rod's angle velocity curves, c) rod's angle acceleration curves, d) slider's linear displacement curve, e) slider's linear velocity curve, f) slider's linear acceleration curve.*

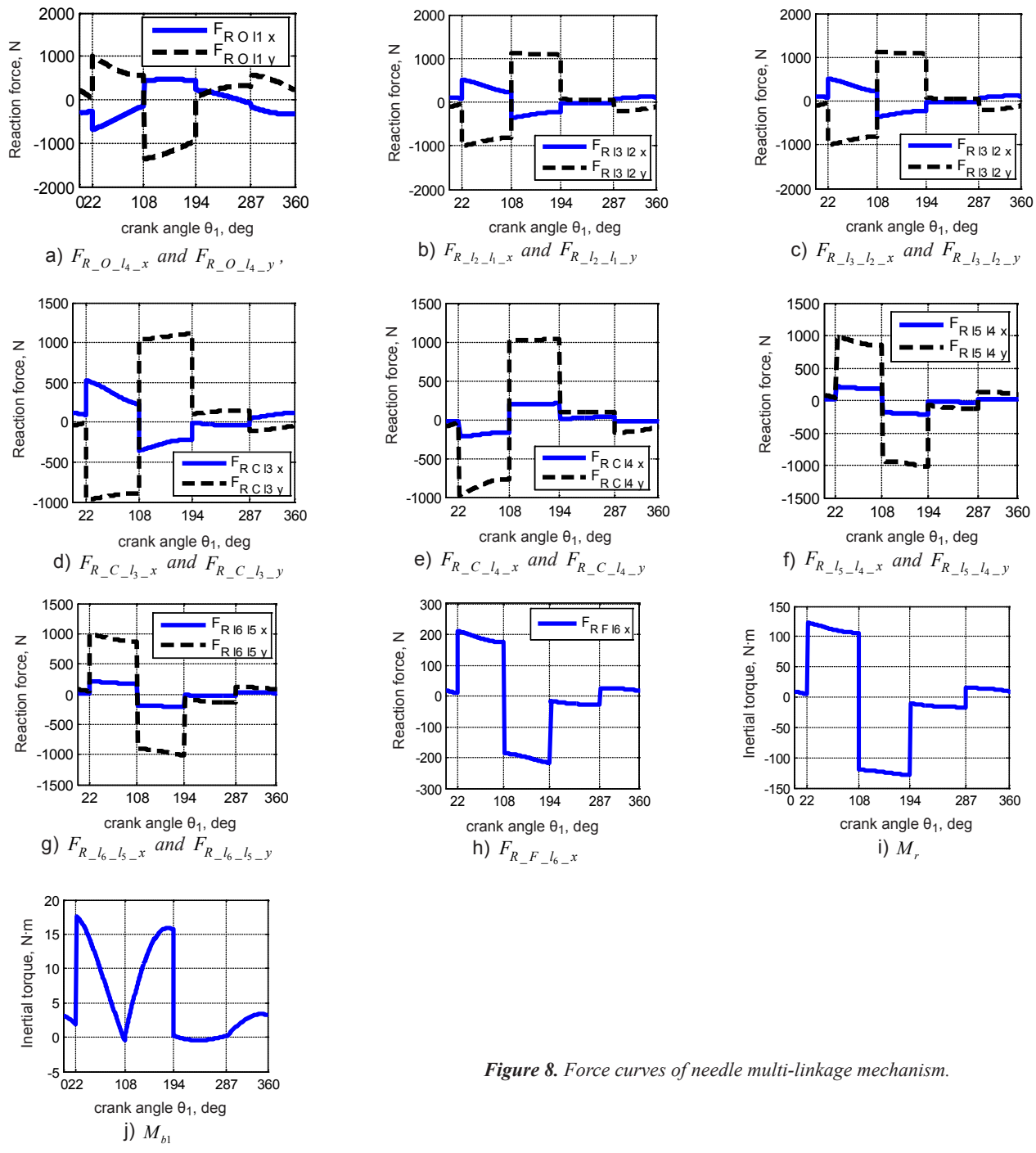

Figure 8. *Force curves of needle multi-linkage mechanism.*

Dynamic characteristic analysis

Focusing on tufting carpet machine type DHGN801D-400, the dynamic characteristics of the needle multi-linkage mechanism is simulated using the model above. The main parameters of the needle multi-linkage mechanism are shown in ***Table 1*** (see page 107). Assume the friction force F_r = 1000 N when the tufting needle moves on the backing and friction force F_r = 1000 N when it moves under the backing. Here, β_1 = 168°. The motion and force curves of the needle multi-linkage mechanism are shown in ***Figure 7*** (see page 107) and ***Figure 8***, respectively.

Analysing ***Figure 7***, it is noted that the range of rotation angle θ_2 is from 101.7° to 114.3° when the main shaft rotates one circle. The tufting needle stroke is about 33 mm. The range of θ_3, θ_4 and θ_5 is, respectively, within 184.3° - 199.4°, -7.89° - 7.38° and 257.9° - 258.5°. From , it is clear that the motion curves of the needle multi-linkage mechanism are smooth and have only a little shock on the whole mechanism. These data are consistent with the actual running ones of tufting carpet machine type DHGN801D-400.

Analysing ***Figure 8***, it is noted that the inertial forces and inertial torque produced by the needle multi-linkage mechanism are an alternating load. When the rotation angle of the main shaft is about 22 degrees, the tufting needle just moves downward to stab the backing.

When the main shaft rotates 108 degrees, the tufting needle arrives at the lowest point. Starting from 109 degrees, the tufting needle moves upwards. When the rotation angle of the main shaft is about 194 degrees, the tufting needle just moves upward to stab the backing. The tufting needle arrives at the highest point until the rotation angle of the main shaft is 287 degrees. Then the tufting needles will continue to move up and down together and repeat this process. From ***Figure 9***, it is clear that the torque that the driven shaft of the needle multi-linkage mechanism suffered is far greater than that on the main shaft. Therefore it is more important to study the effect of alternating loading on the driven shaft of the needle multi-linkage mechanism than thaton the main shaft.

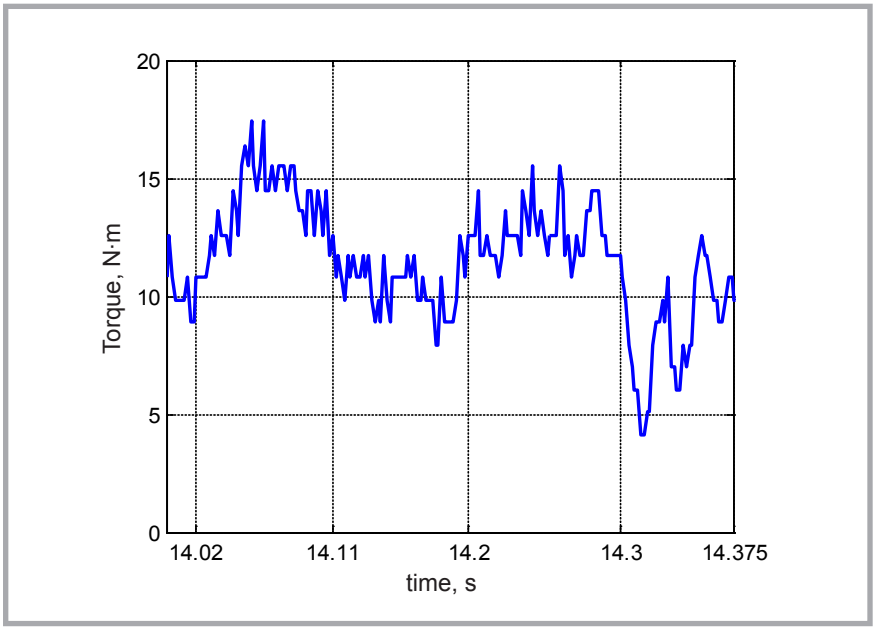

Figure 9. *Experimental result of balancing torque.*

Experiment

To demonstrate the correctness of the theoretical analysis of the needle multi-linkage mechanism, experimentally validation was performed on a tufting carpet machine type DHGN801D-400. Wireless torque sensor DH5905 was applied for measuring the balancing torque of needle the multi-linkage mechanism. The sampling frequency was set to 500 Hz and the rotation speed of the main shaft was 160 r.p.m. Here, the main shaft rotating one circle takes 0.375 seconds. The balancing torque of the needle multi-linkage mechanism can be obtained as shown in ***Figure 9***.

Analysing ***Figure 9***, it is noted that the tufting needle just moves downward to stab the backing when the main shaft rotates to 22 degrees (14.02 s). When the main shaft rotates to 108 degrees (14.11 s), the tufting needle arrives at the lowest point. The tufting needle moves up to stab the backing when the main shaft rotates to 194 degrees (14.20 s). The tufting needle arrives at the highest point until the main shaft rotates to 287 degrees (14.30 s). When the main shaft rotates to 360 degrees (14.375 s), one cycle is over. Compared with ***Figure 8.j*** and ***Figure 9***, it is noted that the experimental result of the balancing torque coincides with simulation results in the previous section. In the process of simulation, due to the friction force F_r chosen according to experience, the experimental result of the balancing torque is not able to totally identically equal to simulation results.

Conclusions

In this work, it was found that the inertia forces and inertia torque acting on needle driven shaft are much greater than that acting on the main shaft. It is more important to study the effect of alternating loading on the driven shaft of the needle multi-linkage mechanism than to study that on the main shaft.

Acknowledgements

This paper was supported by the National Natural Science Foundation of China (Grant No. 51175075).

References

1. Xue Shixin. *Machine-made carpet*. Chemical Industry Press. 2003. 12.
2. Karl-Heinz Erren, Regina Grewe, Robert Heidhues, Frank Hoppner: *Tufting Carpet*, U.S. Patent: USP5494723. 1994.
3. Kathyrn Wise. The carpet industry-covering the future. *American dyestuff reporter*. 1997, 86(6):15-16,18, 21.
4. Gäbl Rainer. New trends and possibilities of double carpet weaving. *Melliand textilberichte-international textile reports*. 2005, 86(11/12): 182-185.
5. Card R T, Card J L. *Tufting machine needle bar drive-comprises bar push rods with individual crank mechanisms actuated from main shaft*, U.S. Patent: US4586445. 1986.
6. Beatty P, Neely M A. *Tufting machine for high speed operations-has paired opposite throw connecting rods for dynamic balance of machine*, U.S. Patent: US5287819. 1994.
7. Price HB. *Tufting machine-has each needle holder between and selectively connectable to limbs of yoke on pushed rod*, U.S. Patent: US 4815402. 1989.
8. Beasley M. *Tufting machine needle bar connecting rod drive cam-comprises upper and lower halves securable about drive shaft*, U.S. Patent: US 5320053. 1993.
9. Roy TC, Rodney EH. *Needle bar foot construction for multiple needle skip-stitch tufting machine*, U.S. Patent: US3978800. 1976.
10. Meng Zhuo, Sun Jingjing, Zhou Tingze, et al. Research on the infuluence that stop position of carpet tufting machine to yarn tension and the method of eliminating stop mark. *Key Engineering Materials*. 2008, 724-728.
11. Xu Yang, Sun Zhijun, Meng Zhuo, Sun Yize, Chen Guangfeng. Research on yarn tension modeling in carpet tufting equipment system. *Journal of Manufacturing Science and Engineering-Transactions of the ASME*, ASME. 2011, 133(3): 031002.1-031002.4.
12. Sun Huan, Chen Zuomo, Ge Wenjie. *Theory of machanies and mechanisms*. Higher Education Press. 2005.12.
13. Li Bincheng, Xu Chao. *Mechanical principle analysis based on Matlab*. Chemical Industry Press. 2010. 10.

Received 05.08.2014 Reviewed 07.07.2015